The micro-Broadband Receiver (uBBR) on the Very-Low-Frequency Propagation Mapper (VPM) CubeSat

Robert Andrew Marshall[1], Austin Patrick Sousa[2], Riley Reid[1], Gordon R. Wilson[3], Michael J Starks[3], Daniel Ramos[3], John Otto Ballenthin[4], Steven Quigley[3], Ronald Kay[5], James Patton[3], Joseph Coombs[3], Judy A. Fennelly[6], Ivan Linscott[7], and Umran S Inan[8]

[1]University of Colorado Boulder
[2]University of Colorado, Boulder
[3]Air Force Research Laboratory
[4]Air Force Research Lab
[5]ATA Aerospace
[6]AFRL
[7]Stanford University
[8]Stanford University, USA

November 21, 2022

Abstract

The Very Low Frequency (VLF) Propagation Mapper (VPM) is a 6U CubeSat designed to measure VLF radio waves in Low-Earth Orbit. The science goals of the VPM mission are to measure VLF signals broadcast by the DSX mission, and to study natural and anthropogenic signals (from lightning and VLF transmitters) in the near-Earth space environment. The primary payload consists of an electric field dipole antenna deployed to 2 meters in length, and a magnetic search coil deployed 50 cm from the spacecraft. Signals from these two sensors are conditioned by analog electronics, sampled, and then processed digitally into downloadable data products. The VPM mission was launched in January 2020; science operations began in March 2020 and continued through September, when contact with the spacecraft was lost. This paper describes the mission goals and instrument designs in detail, as well as some examples of the VPM dataset.

The micro-Broadband Receiver (μBBR) on the Very-Low-Frequency Propagation Mapper (VPM) CubeSat

Robert A. Marshall[1], Austin Sousa[1], Riley Reid[1], Gordon Wilson[2], Michael Starks[2], Daniel Ramos[2], John Ballenthin[2], Steven Quigley[2], Ron Kay[2], James Patton[2], Joseph Coombs[2], Judy Fennelly[2], Ivan Linscott[3], and Umran S. Inan[3,4]

[1]Ann and H. J. Smead Department of Aerospace Engineering Sciences, University of Colorado Boulder, Boulder, CO, USA
[2]Space Vehicles Directorate, Air Force Research Lab, Kirtland AFB, Albuquerque, NM, USA
[3]Department of Electrical Engineering, Stanford University, Stanford, CA, USA
[4]Department of Electrical Engineering, Koç University, Istanbul, Turkey

Key Points:

- The VPM CubeSat was designed to measure VLF waves from Low Earth Orbit
- We present the VPM instrumentation suite, consisting of an electric field dipole antenna, a magnetic search coil, and a data processing unit
- We present example data from the VPM flight mission, demonstrating the capability of the μBBR receiver

Corresponding author: Robert Marshall, `robert.marshall@colorado.edu`

Abstract

The Very Low Frequency (VLF) Propagation Mapper (VPM) is a 6U CubeSat designed to measure VLF radio waves in Low-Earth Orbit. The science goals of the VPM mission are to measure VLF signals broadcast by the DSX mission, and to study natural and anthropogenic signals (from lightning and VLF transmitters) in the near-Earth space environment. The primary payload consists of an electric field dipole antenna deployed to 2 meters in length, and a magnetic search coil deployed 50 cm from the spacecraft. Signals from these two sensors are conditioned by analog electronics, sampled, and then processed digitally into downloadable data products. The VPM mission was launched in January 2020; science operations began in March 2020 and continued through September, when contact with the spacecraft was lost. This paper describes the mission goals and instrument designs in detail, as well as some examples of the VPM dataset.

Plain Language Summary

The Very Low Frequency (VLF) Propagation Mapper (VPM) is a 6U CubeSat designed to study radio signals from lightning, ground-based transmitters, and space-based transmitters and how these signals propagate through the Earth's ionosphere and magnetosphere. This paper describes the mission goals and instrument design; the instrument onboard VPM includes an electric field sensor and a magnetic field sensor. Preliminary data is presented to give a first taste of the VPM dataset. The VPM mission was launched in January 2020; science operations began in March 2020 and continued through September, when contact with the spacecraft was lost.

1 Introduction

Very-low-frequency (VLF, 3–30 kHz) electromagnetic waves are prevalent in near-Earth space, and are produced by a variety of space-based and ground-based sources. Lightning and VLF transmitters launch powerful waves that propagate through the Earth's ionosphere and into the magnetosphere. Within the magnetosphere, naturally-occurring and locally-generated waves include chorus, hiss, and electromagnetic ion-cyclotron (EMIC) waves. Each of these whistler-mode waves propagating in the magnetospheric plasma can induce pitch-angle scattering and precipitation of trapped energetic particles (e.g. Imhof et al., 1983; Inan & Carpenter, 1987). For example, Abel and Thorne (1998) concluded that VLF waves radiated from both lightning and ground-based VLF transmitters play a significant role in maintaining the slot region of depleted fluxes between the inner and outer radiation belts. Each of these waves occurs in different regions of space, and with different amplitudes and frequencies, and therefore each affect somewhat different populations of energetic particles.

The propagation of these VLF waves within the magnetosphere, as well as from the ground through the ionosphere, is complex and difficult to experimentally assess. Chorus and hiss waves, for example, are regularly measured by spacecraft such as the Van Allen Probes, but without knowledge of the source region of these waves, the propagation characteristics are difficult to characterize. Propagation characteristics such as the propagation direction, amplitude decay and/or growth, and reflections within the magnetosphere, are critical to understanding the quantitative effect these waves have on energetic particles.

Two methods are investigated to better understand the propagation of these VLF waves. First, a satellite can measure the waves launched from the ground by lightning and/or VLF transmitters; with knowledge of the signal source, and some idea of the propagation path (i.e. through the ionosphere), the propagation characteristics can be determined. Second, artificial waves can be launched from within the magnetosphere with known amplitude, polarization, and frequency, and measured at a second point in space; again, with knowledge of the source location and wave characteristics, the propagation characteristics can be determined.

The Very-low-frequency Propagation Mapper (VPM) is designed for both of these experimental scenarios. From low-Earth orbit (LEO), VPM was designed to measure natural and anthropogenic signals transmitted from the ground through the ionosphere, as well as signals broadcast from the inner magnetosphere by the Demonstration and Science Experiments (DSX) mission. In this paper we provide a brief overview of the VPM mission and spacecraft design; however, the focus of this paper is on the design of the compact VLF receiver on VPM, which is denoted the micro-broadband receiver, or μBBR. The VPM mission and instrumentation was previously described in (Ramos et al., 2019); in this paper, we provide a more in-depth description of the instrument details, as well as the first data from the mission.

1.1 Recent VLF Missions in LEO

The past 20 years have seen only a few VLF receivers in LEO. The DEMETER mission (Parrot, 2002) was designed to study ionospheric perturbations due to seismic activity, as well as general global study of the electromagnetic environment in LEO. The mission included the Instrument Magnetic Search Coil (IMSC), a set of three orthogonal search coils (Parrot, 2006), as well as the Instrument Champ Electrique (ICE), which measures three orthogonal components of electric field using four spherical probes (Berthelier et al., 2006). The IMSC covers the frequency range up to 20 kHz, while ICE covers up to 3.175 MHz; however the VLF data products cover the common range up to 20 kHz.

The DEMETER mission lasted from launch in June 2004 until retirement in December 2010. A great number of VLF science results have come from this mission, including observations of radiation belt precipitation due to VLF transmitters (Sauvaud et al., 2008); assessment of VLF transmitter propagation into the magnetosphere (Starks et al., 2008; Cohen & Inan, 2012; Cohen et al., 2012); observations of ionospheric heating by VLF transmitters (Bell et al., 2011); as well as numerous results relating VLF observations to seismic activity (e.g., Molchanov et al., 2006; Píša et al., 2013). Of special interest, Parrot et al. (2015) provides an overview of numerous unusual and unique VLF observations during the DEMETER mission.

The CASSIOPE mission (Yau & James, 2011) was launched in 2013 and continues to operate. While the mission of the Enhanced Polar Outflow Probe (E-POP) is to observe plasma processes in the polar ionosphere, the mission carries a Radio Receiver Instrument (RRI) (James et al., 2015) with bandwidth from 10 Hz to 18 MHz, thus covering the entire VLF band. Some published results on VLF waves include measurements of VLF waves in the topside ionosphere (James & Yau, 2019), and recent observations of VLF wave amplification from artificially-injected plasma (Bernhardt et al., 2021).

More recently, the Chinese Seismo-Electromagnetic Satellite (CSES), also known as ZhangHeng-1 or ZH-1, was launched in 2018 (Shen et al., 2018). Similar in both objectives and instrumentation to DEMETER, the ZH-1 mission carries the electric field instrument EFD (Huang et al., 2018) and a search coil magnetometer (SCM) instrument; these two instruments have bandwidth identical to the instruments on DEMETER. Some of the early results from ZH-1 include studies of VLF transmitter signals (Zhao et al., 2019), and of the relationship between VLF waves and electron precipitation from the radiation belts (Zhima et al., 2020).

DEMETER was a microsatellite with a spacecraft mass of 130 kg, and CASSIOPE and ZH-1 are both small satellites with spacecraft mass of 500 kg and 700 kg, respectively. VPM, on the other hand, is a 6U CubeSat with a total spacecraft mass of less than 12 kg. As such, VPM is the first mission to successfully fly a VLF receiver on a Cube-

Sat. VPM serves as a pathfinder mission, demonstrating the ability to make high-SNR measurements of VLF waves in LEO and to conduct valuable scientific investigations from a CubeSat.

1.2 The VPM Mission

The VLF Propagation Mapper (VPM) CubeSat was conceived primarily as a complement to the Air Force Research Laboratory (AFRL)'s Demonstration and Science Experiments (DSX) mission (Scherbarth et al., 2009), and in particular the onboard Wave Induced Precipitation of Electron Radiation (WIPER) experiment. WIPER on DSX includes a VLF transmitter that broadcasts waves using a 80-m dipole antenna (Spanjers et al., 2006). Depending on the wave launch location in the magnetosphere and the transmitted frequency, these waves may be able to reach LEO. The VPM mission, therefore, is to measure DSX-broadcast VLF waves and characterize the radiation pattern and efficiency of the DSX antenna as well as the propagation of these waves between DSX and LEO.

In addition to DSX observations, VPM has secondary goals to measure natural and anthropogenic VLF signals in low-Earth orbit, including lightning-generated whistlers and ground-based VLF transmitters. Such measurements have been made previously by missions such as DEMETER (Parrot, 2002); VPM will thus contribute to the long-term record of VLF waves in LEO. With complementary ground based VLF measurements, detailed studies are planned to characterize the transionospheric propagation of signals from the ground, as well as the propagation through the inner magnetosphere to the conjugate region.

Figure 1 illustrates the VPM mission concept along with DSX and ground-based transmitters. VPM is orbiting in LEO at about 500 km altitude; VLF waves launched by DSX propagate as whistler-mode waves in the magnetized plasmasphere, and are largely guided by the Earth's magnetic field lines. When the two spacecraft make a magnetic conjunction, i.e. are found on the same magnetic field line, there is a good probability that VPM will measure the waves transmitted by DSX. The measurement on VPM will then be used to assess the amplitude of those DSX transmissions, and look for signatures of wave growth.

2 VPM Instrumentation

The VPM payload consists of a single electric field dipole antenna and a single magnetic field search coil antenna. Each of these sensors has an associated preamplifier, and the signals from the preamps are then fed to the analog receiver, which includes a low-noise amplifier (LNA) and an anti-aliasing filter (AAF). From there, the signal goes through a selectable high-pass filter (HPF) with a 3 kHz cutoff, designed to attenuate noise at the lowest frequencies if present. Another selectable gain stage follows, with an optional gain of 10, and then the signal is fed to an ADC. Data from the ADCs is fed to an FPGA, where onboard data processing occurs. Figure 3 shows a graphical block diagram of the electronics.

Figure 4 shows the card stack that makes up the payload electronics. Each board is approximately 9 × 9 cm, with a 4 × 4 cm cutout region, designed to accommodate the search coil deployer. The analog receiver (the μBBR) takes up two boards on the top of the stack; each board includes the PARX LNA chip, the PARX ADC chip, switches for the gain and filter selection, and a stack connector that connects to the other boards for power and data transfer. The Data Processing Unit (DPU) board primarily houses the FPGAs for data processing, SRAM memory, and connectors to the spacecraft bus. The Interface (INT) board contains power conditioning circuitry and houses the Novatel OEM719 GPS receiver board.

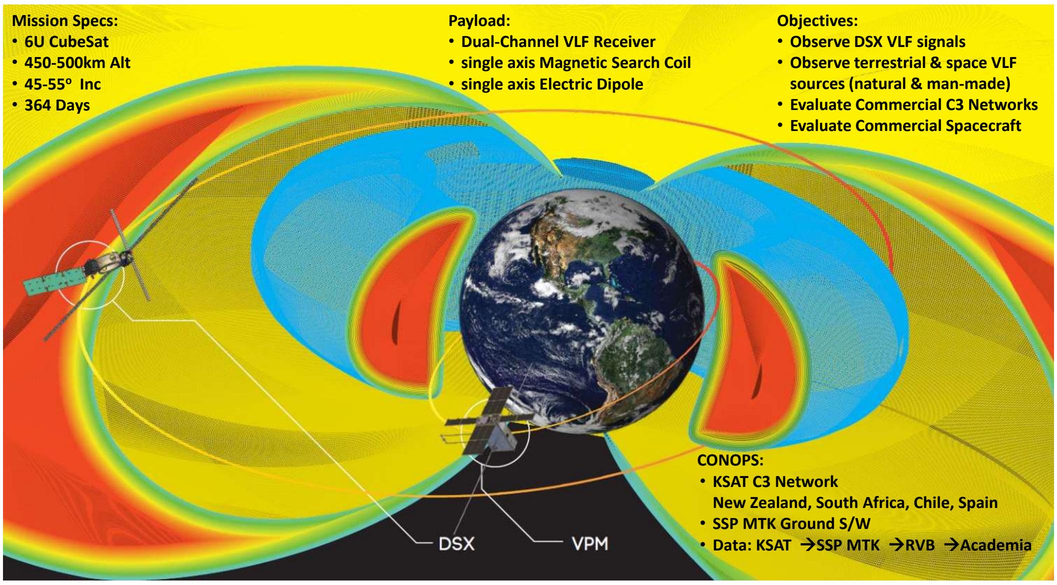

Figure 1. Schematic diagram of the VPM mission in LEO, with the complementary DSX mission in MEO.

2.1 E-field Sensor

The Dipole Antenna Assembly (DAA) consists of two quasi-bistable 1-meter tape springs coiled and stowed in a deployment housing, shown in Figure 5. The doors that constrain the tape springs are restrained by a Spectra cord that is routed over a NiChrome heating element (burn wire). When sufficient current passes through the NiChrome wire, it heats up to the point where the Spectra cord melts, releasing the doors and allows the tape springs to unroll to their full length. The system that supplies the current to the NiChrome wire is programmed to apply unregulated spacecraft battery voltage to the burn wire circuit for five seconds. This time interval is programmed into the payload firmware; based on previously performed burn wire tests, this duration is longer than the time needed to burn through the Spectra cord. Resistance in the burn wire circuit is adjusted so that the appropriate current flows in the NiChrome wire to assure that the Spectra cord melts within that time interval. Once the antenna is deployed, the burn wire circuit is no longer active and becomes a passive component for the duration of the mission.

The signal from each of the two E-field monopole antennas is fed to a single-ended low-noise preamplifier. The amplifier is centered around a low-noise JFET-input op-amp (OP215S) in a non-inverting amplifier configuration, providing a voltage gain of $\sim$82. Together with the gain of 10 in the low-noise amplifier (Section 2.3), and assuming an effective antenna length of 1.1 m, the overall gain of the E-field channel is $\sim$900.

2.2 B-field Sensor

The VPM search coil was provided by the Laboratoire de Physique et de Chimie de l'Environnement et de l'Espace (LPC2E) in Orléans, France. It is a variation of heritage designs flown on DEMETER (Parrot, 2006) and other missions. The search coil antenna is 124 mm long, 14 mm in diameter, and weighs 42 grams. It includes 12,600 turns of 80 μm enameled copper wire for the primary coil, and 29 turns of the same wire for the secondary coil. The antenna is connected to a preamplifier circuit through a 63 cm cable, utilizing a shielded, twisted triplet of 28 AWG wires. The preamp, also provided by LPC2E, is installed within the main spacecraft bus.

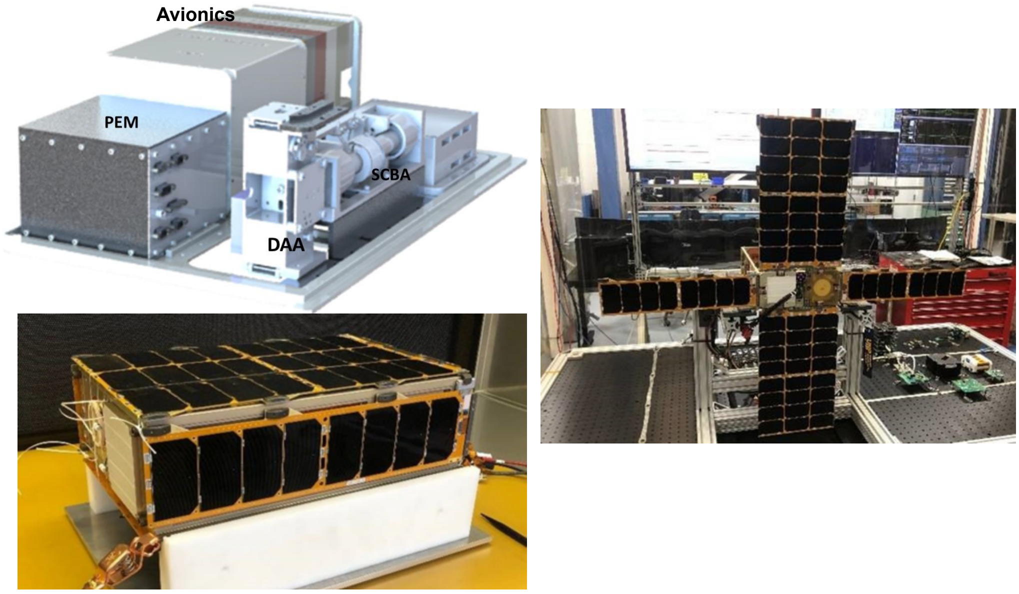

Figure 2. top left: CAD rendering of VPM internal components. Bottom left: The completed VPM spacecraft is the stowed configuration. Right: The completed VPM spacecraft with solar panels deployed.

The magnetic search coil is mounted on two quasi-bistable tape springs that are attached to the search coil boom assembly (SCBA) as shown in Figure 6 (left). The tape springs are 50 centimeters in length and are connected so that when the search coil is released, the tape springs unroll parallel to each other and move the search coil 50 cm away from the body of the spacecraft. The search coil is restrained in the SCBA saddles by a Spectra cord. Like the DAA, this cord is routed over a NiChrome wire which melts the cord and allows the tape springs to unroll and extend the search coil away from the body of the spacecraft.

Figure 6 (right) shows the search coil response and sensitivity curves versus frequency; note that the gain includes the amplification and frequency response of the preamplifier circuit. Between the design frequencies of 300 Hz to 30 kHz, the gain varies between 7–16 dB V/nT, and the sensitivity is well below 10^{-4} nT/$\sqrt{\text{Hz}}$.

The search coil is connected to the preamplifer by a shielded, twisted triple cable; the cable is wound around the search coil prior to deployment, as shown in Figure 6, and is rolled out with the search coil when deployed. The search coil preamplifier was also provided by LPC2E, and follows the basic design topology used on DEMETER and other missions (Parrot et al., 2006).

2.3 Instrument Analog Electronics: The μBBR

Signals from both the E-field and B-field preamplifiers are routed to a stack of electronics known as the Payload Electronics Module, or PEM. Within the PEM are four electronics boards: two boards make up the micro-Broadband Receiver (μBBR); one board comprises the Data Processing Unit (DPU); and an Interface board (INT) houses the GPS receiver, power regulators, interfaces to the spacecraft bus, and interfaces to the deployment electronics.

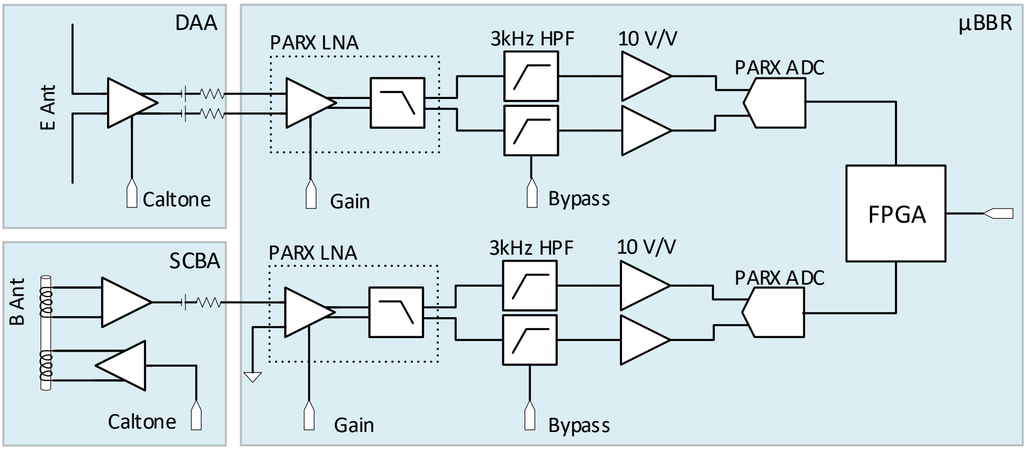

Figure 3. Micro-broadband receiver (µBBR) electronics block diagram, from sensors (left) to FGPA data processing (right).

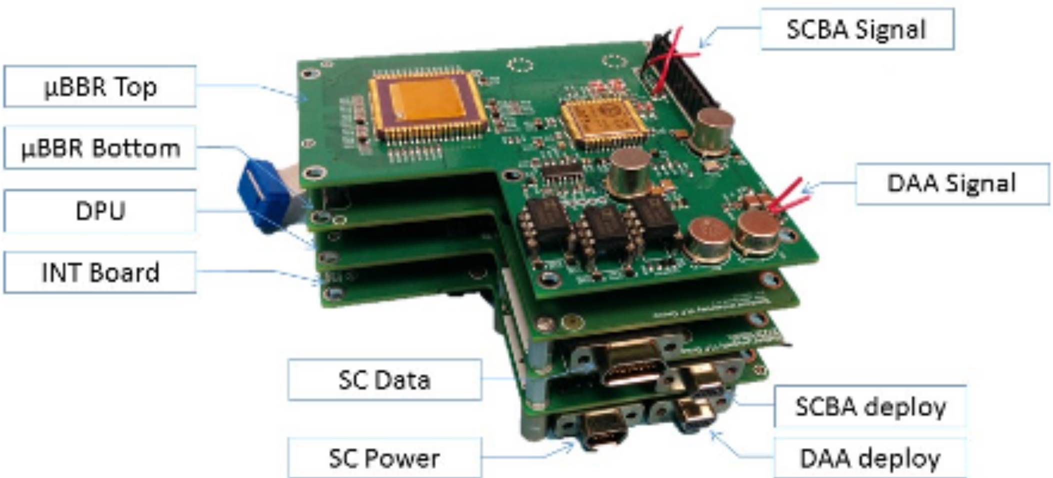

Figure 4. µBBR instrument electronics stack, consisting of the two µBBR receiver boards, DPU board, and interface board, which includes a Novatel OEM719 GPS receiver. The boards are approximately 9 cm square, with a 4 cm square cutout.

Analog signals first enter the µBBR via pigtails, shown on the top of the stack in Figure 4, and are routed through a selectable gain stage, with a gain of either 1 or 10, and then to the PARX low-noise amplifier (LNA) and anti-aliasing filter (AAF) chip. These two circuits reside on the same custom chip first developed by (Mossawir et al., 2006) for the DSX mission. The LNA/AAF is a fully differential amplifier and anti-aliasing filter, designed for space readiness, with ∼90 dB dynamic range over the VLF range. It includes a selectable gain setting, allowing 10 dB of variation. From the LNA/AAF, the signal is next passed to a switchable high-pass filter with a 3 kHz cutoff. This filter was designed to reduce spacecraft noise, DC bias, and/or chorus and hiss signals that might saturate the receiver in its high-gain setting. Next, the signal passes through an amplifier stage with a fixed gain of 10, and then enters the PARX ADC. The ADC is another chip developed specifically for DSX and other space missions by (Wang, 2009). For VPM,

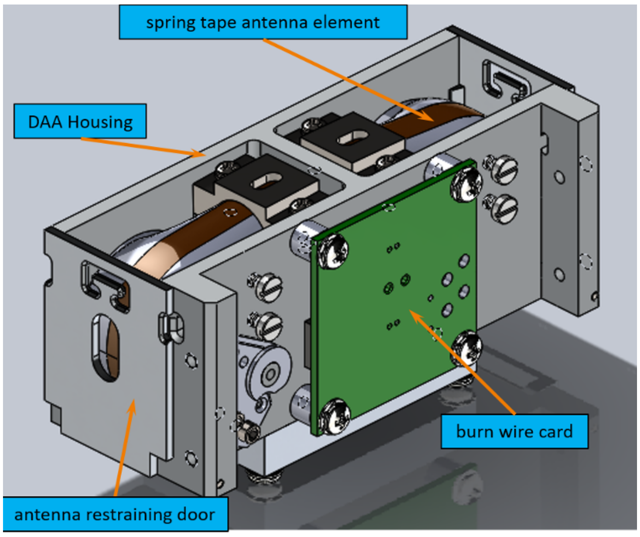

Figure 5. CAD model of VPM electric field antenna in its deployer. The antenna itself is the conductive copper-colored element on the grey tape spring just visible inside the housing.

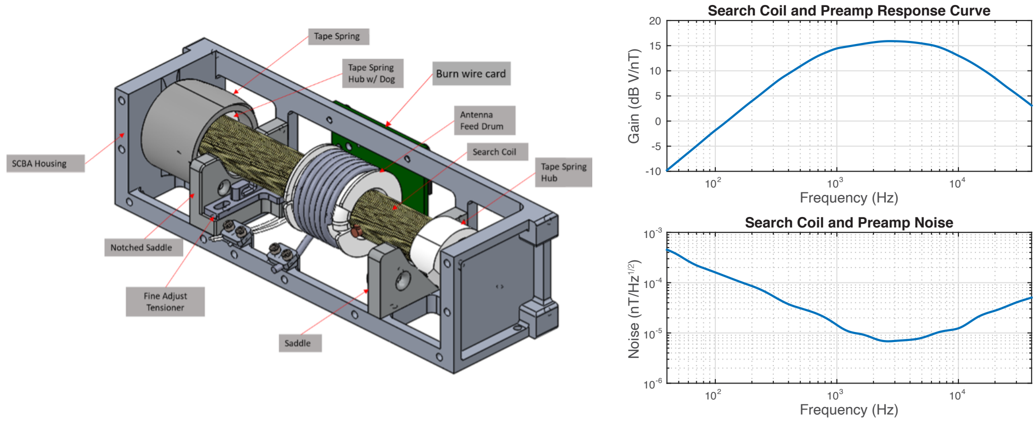

Figure 6. VPM magnetic field search coil boom assembly (SCBA); search coil gain response and sensitivity curves.

it is set to sample both signals at 80 kS/s with 16-bit resolution. Finally, the digital signal enters the FPGA for digital processing.

2.4 Instrument Data Processing

The Data Processing Unit (DPU) is designed primarily around a Microsemi ProASIC3 FPGA. The processing chain within the DPU is depicted in Figure 7. The DPU provides two primary data products: a survey product, and burst products. The survey mode runs constantly in the FGPA. First, FFTs are computed from the time-domain signals; VPM uses 1024-point FFTs with 512-point overlap and a 1024-point windowing function. FFTs are then accumulated over a programmable time duration of either 6.5536, 13.1072, or 26.2144 seconds (corresponding to 1024, 2048, or 4096 accumulated FFTs). The result is then compressed with $\log_2$ scaling, and then survey products are assembled, packetized with CCSDS header information, and sent to the SRAM memory.

The burst mode has more options. VPM can produce time-domain or frequency-domain bursts; the latter provide the raw FFTs before they are averaged in the survey product. Burst mode also includes time-windowing; through a command, the mission operator can select a temporal sequence such as 5 seconds on / 5 seconds off for 60 seconds. Frequency-windowing allows the operator to select specific sets of frequency bins from the FFT outputs. These options enable longer duration bursts for the same total data volume, or allow the user to focus on specific frequencies of interest, for example during a DSX transmission at a known frequency. Time-domain data can also be decimated to a lower sampling rate; when this option is selected, the data is first passed through a pre-defined digital FIR filter and then resampled at the desired rate. All of the available options are set via a 24-bit command to the DPU. Finally, burst products are similarly packetized with CCSDS and then sent to the local SRAM memory.

The DPU includes a space-rated 1 Gb SRAM memory chip from 3D-Plus; the memory controller is implemented in the FPGA. When requested from the spacecraft, data is transferred over an RS422 interface and stored in the spacecraft recorder.

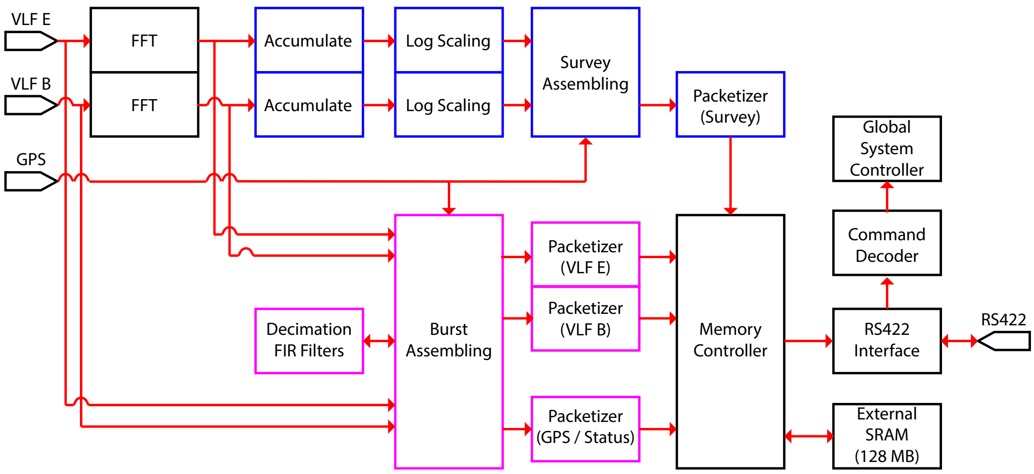

Figure 7. FPGA processing chain within the DPU. VLF channels are processed through survey (blue) and burst (magenta) chains, and then stored in memory and transmitted to the spacecraft on-board storage.

2.5 Calibration

The µBBR signal chain features an onboard calibration signal generator, which can be used to assess the frequency response of the system on-orbit. A pseudorandom digital signal is generated using the µBBR FPGA, using the feedback register methodology described by (Paschal, 2005). VPM uses a 7-bit feedback register for a maximal-length sequence of 128 samples. This signal is passed through a voltage divider and capacitively-coupled to the input of each analog channel. The Fourier transform of the resulting signal features a comb of uniformly-spaced frequencies, as shown in Figure 8. When calibration mode is entered, the system will generate one minute of calibration tone, which can be recorded by a 30-second, full-resolution burst.

In addition, an onboard digital sine-wave generator can be enabled; in this mode the µBBR ignores any analog signal and delivers a full-scale sine wave. While not scientifically useful, this mode enables diagnosis of communications issues, and confirmation of survey-mode processing.

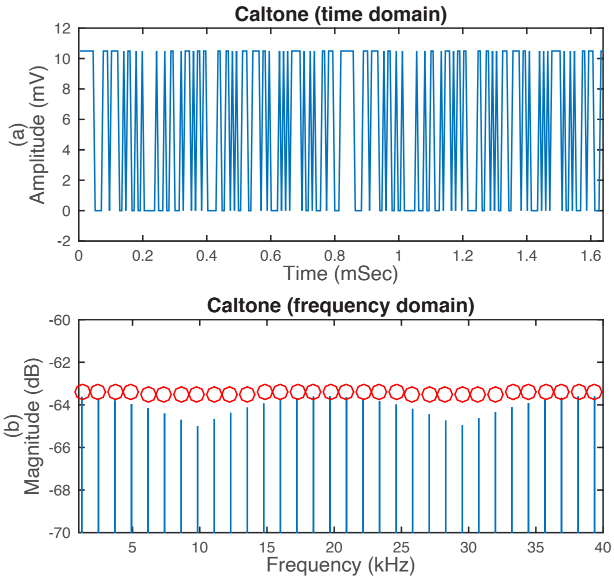

Figure 8. Top: Time-series of the calibration tone applied to both E and B channels. Bottom: Fourier transform of this signal, showing the comb spectrum.

3 Mission Summary

The VPM spacecraft was launched to the International Space Station (ISS) on December 5, 2019 on a SpaceX Dragon resupply flight. After storage on the ISS for about 50 days, it was installed on the slingshot deployer on the hatch of the Cygnus resupply vehicle. On January 31, 2020, the Cygnus vehicle separated from the ISS and raised its orbit to 475 km. On February 1, 2020, the VPM spacecraft was deployed into a near circular orbit at this altitude and 51.6 degree inclination.

Commissioning of the spacecraft followed, including deployment of solar panels, electric field antennas, and the magnetic field search coil. Of particular interest, the electric field antennas were deployed on March 6, 2020. Burst mode data was collected during the time of deployment, and an abrupt change in signal intensity was seen in burst data collected during the deployment. In addition, High-rate data from the inertial measurement unit (IMU) collected by the ADCS system indicated that a brief jitter of the spacecraft occurred at the same moment. These two factors confirmed the successful deployment of the dipole antenna.

The search coil deployment was first attempted on March 10, 2020; burst mode data was collected during the time of deployment, but high-rate IMU data was not collected. There was no change in the data quality before and after deployment, and it was too noisy to observe any natural signals. Multiple deployment attempts were made over the next few months, with no change in signal quality. The magnetic field data has thus been unusable for the duration of the mission.

However, high quality electric field data has been collected starting from mid-March 2020, and through mid-September 2020. Survey data was collected continuously, though not all data was brought to the ground. Burst data has been collected during scheduled events of interest (i.e. conjunction events) in typically 30 or 60 second bursts.

On September 1, 2020, the ground lost the ability to communicate with the VPM spacecraft. Ground-based imaging provided evidence that the spacecraft was tumbling out of control. Further attempts to communicate with the spacecraft were unsuccessful.

4 Example Data

Roughly six months of data were collected by the VPM electric field channel. The dataset includes survey data throughout the mission (though not all data was brought to the ground). Numerous burst events were collected, most corresponding with conjunction events with other spacecraft or ground transmitters. In this section we provide some example data to demonstrate the functionality and capability of the μBBR receiver.

4.1 Survey Data

Figure 9 (right) shows example survey data from June 28, 2020, covering a three-hour window of data (roughly two orbits). The left panels show the orbit information over this three-hour period: a map of the orbit track (color-coded by time from dark blue to yellow), also showing VLF transmitter locations as red dots; and time-series panels showing the L-shell, altitude, latitude, and longitude of the spacecraft. The L-shell is calculated from the IGRF magnetic field model; the position information is taken directly from the GPS receiver incorporated into the instrument electronics. The bottom two panels show the GPS solution status (0 denotes a complete solution; any other integer implies a bad solution) and a binary day vs. night plot, based on the location of the terminator at the ground.

The data during this time period was collected with the high-gain setting on the analog receiver, and the low-pass filter enabled; the dropoff in the background is evident in the data plot below ∼3 kHz, in particular during periods of low signal activity.

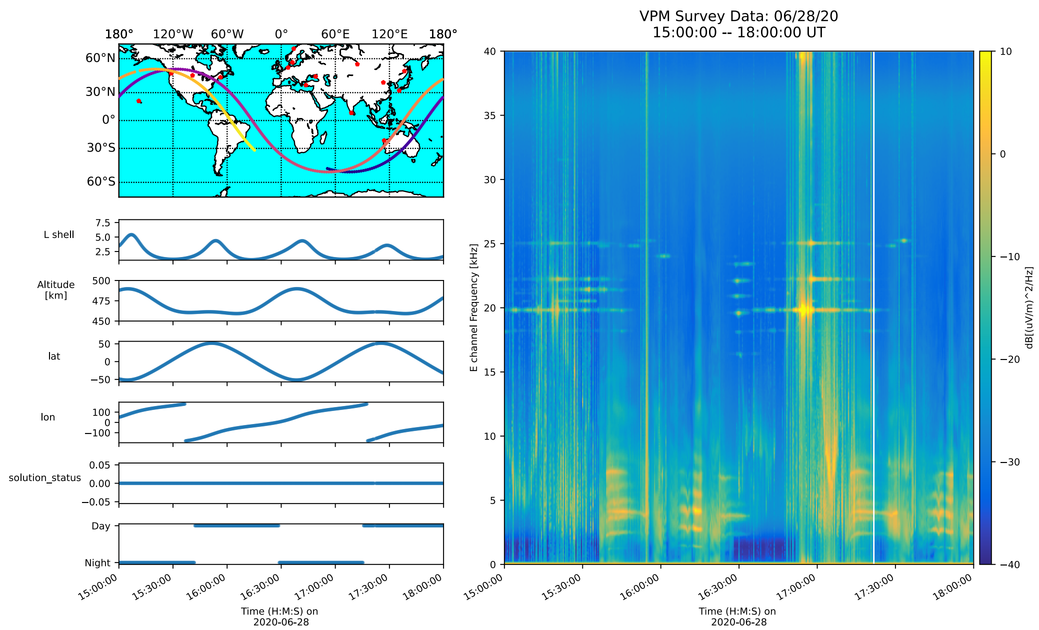

Figure 9. Example Survey data product. Left: map and time-series plots showing the geographic location of the spacecraft throughout this three-hour period. Right: VLF spectrogram covering 0–40 kHz over three hours. See the text for details on each panel and discussion of the data.

Numerous features are evident in the data. First, spacecraft interference is evident between 2–8 kHz. Because these signatures appear only in daytime, they are thought to be related to the solar panel charging system. These signatures limit the usefulness of the daytime data in this frequency range.

During nighttime, there is clear indication of lightning-generated whistler (LGW) activity, indicated by the vertical structure covering all frequencies (these are more evident in the burst data in Figure 10). Numerous VLF transmitters are also evident between ∼20–25 kHz, measured at different times in the orbit. These include the NWC transmitter (Western Australia) at 19.8 kHz; NPM (Hawaii) at 21.4 kHz; NML (North Dakota) at 25.2 kHz; and others. The strength of each VLF transmitter signal depends on the orbit (i.e. the lateral distance between the satellite footprint and the transmitter) and the ionospheric attenuation at the time; it is well known that the ionosphere attenuates ground-based signals during the daytime much more than at nighttime (e.g., Helliwell, 1965; Graf et al., 2013), but there are also finer spatial and temporal variations that are not easily characterized. Just before 17:00 UT, the spacecraft flew almost directly above the NWC transmitter; at this time the signal is so strong in the E-field channel that it approaches saturation, and the second harmonic is evident near 40 kHz.

Between 16:30 and 17:00 UT, this survey example also shows indications of lower hybrid resonance (LHR) oscillations between 8–12 kHz. Other survey data examples show even more prominent LHR oscillations.

4.2 Burst Data

Figure 10 shows an example burst event, from June 14, 2020, starting at 06:59:10 UT. The top left panel shows calibrated time-series data; the top right panel shows the calibrated spectrogram, again covering 0–40 kHz. This burst is an example of the "10 on, 2 off" burst mode, where data is collected for ten seconds, following by a two-second pause, and this pattern repeats for five cycles. The lower panel shows a map of the spacecraft location at the time of the burst; the spacecraft position is indicated by colored circles in the middle of the colored trajectory, which is provided for context. Each of the five colored circle gives the spacecraft location at 12-second intervals, corresponding to each of the five burst collections.

This burst data shows examples of high-quality lightning-generated whistlers over the entire minute of data, with their spectra extending from ∼3 kHz to over 20 kHz; note that the high-pass filter at 3 kHz was on at this time, so whistler energy below 3 kHz, while likely present, is attenuated by the filter. As this is nighttime during the northern hemisphere summer, these are likely whistlers injected by lightning in the conjugate region, i.e. in the United States. Numerous VLF transmitter signals are also evident, again clearly measured in the conjugate region; these include the 24.0 kHz NAA signal, the 24.8 kHz NLK signal, and the 25.2 kHz NML signal, all originating from the continental United States. The NPM signal at 21.4 kHz and the NWC signal at 19.8 kHz are also evident.

Figure 11 shows a zoomed-in view of the data from Figure 10, covering 6 seconds beginning at 6:59:38 UT (in the third 10-second window of Figure 10). This example clearly shows the many prominent whistlers observed at this time, along with the clear and distinct VLF transmitter signals. The dispersion characteristics of these whistlers make it clear that they originated from the conjugate hemisphere. It is also clear that significant whistler energy persists up to ∼35 kHz or more, even for these whistlers that have traversed the magnetosphere.

Numerous other burst events have been captured during the six month successful VPM mission period. Many of these show other whistler and VLF transmitter signatures; LHR oscillations; and a variety of other signatures. The VPM burst data are still be-

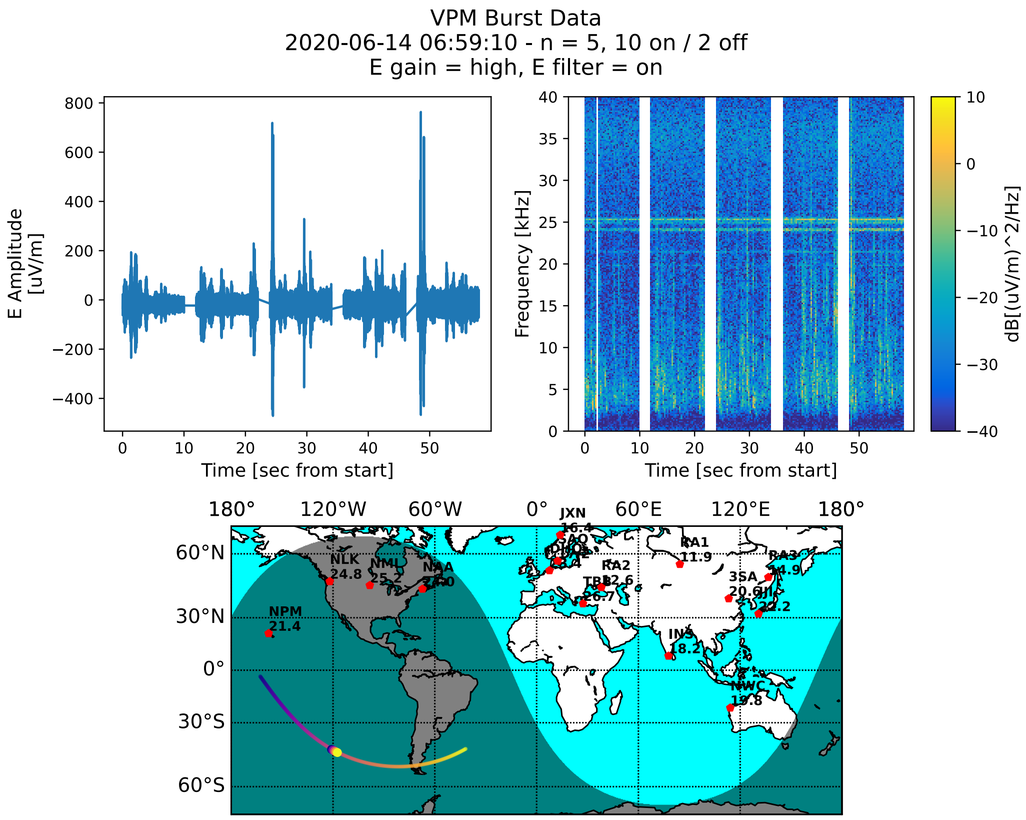

Figure 10. Example Burst data event. Top left: time-series data, sampled at 80 kHz, for a one-minute period. Note the 2-second gaps every 10 seconds as part of the collection mode. Top right: spectrogram of the same data, showing whistler and VLF transmitter activity. Bottom: map showing the spacecraft location over the South Pacific Ocean, in eclipse, approximately magnetically conjugate to North America.

ing analyzed to identify the signal from the DSX transmitter, which is expected to be much weaker than those from terrestrial transmitters. These events and other data will be analyzed in depth in future work.

5 Summary and Conclusions

In this paper we have presented the design and results of the µBBR instrument on the VPM CubeSat mission. The µBBR is a two-channel VLF receiver covering frequencies from 0.3–40 kHz, incorporating one electric field channel and one magnetic field channel. While the magnetic search coil likely failed to deploy, the electric field dipole antenna was successful and collected data for the six-month duration of the VPM mission. Detailed analysis of many aspects of this dataset is currently underway.

VPM serves as a pathfinder mission, as the first CubeSat to successfully fly a science-quality VLF receiver. Future missions will leverage numerous novel aspects of the µBBR design, including the sensors, deployment mechanisms, compact preamplifier circuits, and the compact analog and digital signal processing chain.

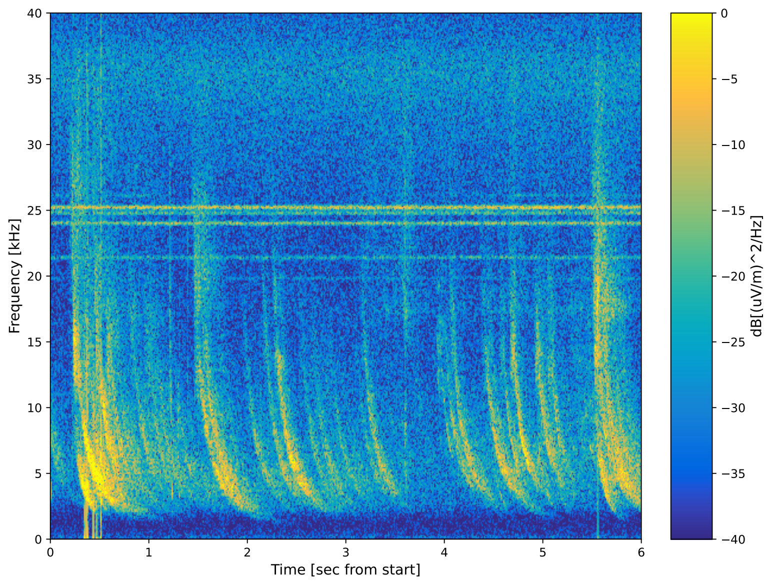

Figure 11. Zoom-in of 6-second period from Figure 10, starting at 6:59:38 UT, and showing evidence of strong whistlers that originated in the conjugate region.

Acknowledgments

This work was supported by the Air Force Research Laboratory. The VPM payload development was conducted under contract FA9453-12-C-0217 to Stanford University. The Air Force Research Laboratory built and operated the VPM spacecraft. We thank LPC2E for providing the search coil for VPM. Payload integration support was conducted by the University of Colorado Boulder under contract NM17-339 from ATA Aerospace. Data processing and analysis was conducted under contract FA9453-19-C-0400 to Atmospheric and Environmental Research (AER), Incorporated and subcontract P2247-04 to the University of Colorado Boulder. The authors wish to acknowledge the many students at Stanford and CU Boulder who contributed to the design, development, and operation of the VPM µBBR instrument; as well as the efforts of the DoD Space Test Program and the AFRL Small Satellite Portfolio to launch and operate the VPM spacecraft.

The data presented in this work are published and available at https://doi.org/10.5281/zenodo.5207962.

References

Abel, B., & Thorne, R. M. (1998). Electron scattering loss in earth's inner magnetosphere: 1. dominant physical processes. *Journal of Geophysical Research: Space Physics*, *103*(A2), 2385–2396.

Bell, T., Graf, K., Inan, U., Piddyachiy, D., & Parrot, M. (2011). Demeter observations of ionospheric heating by powerful vlf transmitters. *Geophysical research letters*, *38*(11).

Bernhardt, P. A., Bougas, W. C., Griffin, M. K., Watson, C., Langley, R. B., Howarth, A. D., ... others (2021). Strong amplification of elf/vlf signals in space using neutral gas injections from a satellite rocket engine. *Radio Science*, *56*(2), e2020RS007207.

Berthelier, J.-J., Godefroy, M., Leblanc, F., Malingre, M., Menvielle, M., Lagoutte, D., ... others (2006). Ice, the electric field experiment on demeter. *Planetary and Space Science*, *54*(5), 456–471.

Cohen, M. B., & Inan, U. S. (2012). Terrestrial vlf transmitter injection into the magnetosphere. *J. Geophys. Res.*, *117*, A08310.

Cohen, M. B., Lehtinen, N. G., & Inan, U. S. (2012). Models of ionospheric VLF absorption of powerful ground based transmitters. *Geophys. Res. Lett.*, *39*, L24101.

Graf, K. L., Lehtinen, N. G., Spasojevic, M., Cohen, M. B., Marshall, R. A., & Inan, U. S. (2013). Analysis of experimentally-validated trans-ionospheric attenuation estimates of vlf signals. *J. Geophys. Res.*.

Helliwell, R. A. (1965). *Whistlers and related ionospheric phenomena*. Stanford University Press.

Huang, J., Lei, J., Li, S., Zeren, Z., Li, C., Zhu, X., & Yu, W. (2018). The electric field detector (efd) onboard the zh-1 satellite and first observational results. *Earth and Planetary Physics*, *2*(6), 469–478.

Imhof, W. L., Reagan, J. B., Voss, H. D., Gaines, E. E., Datlowe, D. W., Mobilia, J., ... Joiner, R. G. (1983). Direct observation of radiation belt electrons precipitated by the controlled injection of vlf signals from a ground-based transmitter. *Geophys. Res. Lett.*, *10*, 361-364.

Inan, U. S., & Carpenter, D. L. (1987). Lightning-induced electron precipitation events observed at L=2.4 as phase and amplitude perturbations on subionospheric VLF signals. *J. Geophys. Res.*, *92*(A4), 3293-3303.

James, H., King, E., White, A., Hum, R., Lunscher, W., & Siefring, C. (2015). The e-pop radio receiver instrument on cassiope. *Space Science Reviews*, *189*(1), 79–105.

James, H., & Yau, A. (2019). Observations of electromagnetic waves at very low frequency in the near topside ionosphere. In *2019 international conference on electromagnetics in advanced applications (iceaa)* (pp. 1452–1452).

Molchanov, O., Rozhnoi, A., Solovieva, M., Akentieva, O., Berthelier, J.-J., Parrot, M., ... Hayakawa, M. (2006). Global diagnostics of the ionospheric perturbations related to the seismic activity using the vlf radio signals collected on the demeter satellite. *Natural Hazards and Earth System Sciences*, *6*(5), 745–753.

Mossawir, B., Linscott, I. R., Inan, U. S., Roeder, J. L., Osborn, J. V., Witczak, S. C., ... LaLumondiere, S. D. (2006). A tid and see radiation-hardened, wideband, low-noise amplifier. *IEEE transactions on nuclear science*, *53*(6), 3439–3448.

Parrot, M. (2002). The micro-satellite demeter. *Journal of Geodynamics*, *33*(4-5), 535–541.

Parrot, M. (2006). Special issue: First results of the DEMETER microsatellite. *Planet. Space Sci.*, *54*(5), 411-558.

Parrot, M., Benoist, D., Berthelier, J., Blecki, J., Chapuis, Y., Colin, F., ... others (2006). The magnetic field experiment imsc and its data processing onboard demeter: Scientific objectives, description and first results. *Planetary and Space Science*, *54*(5), 441–455.

Parrot, M., Berthelier, J.-J., Blecki, J., Brochot, J., Hobara, Y., Lagoutte, D., ... others (2015). Unexpected very low frequency (vlf) radio events recorded by the ionospheric satellite demeter. *Surveys in Geophysics*, *36*(3), 483.

Paschal, E. (2005). *Pseudo-random waveforms and comb calibration signals* (Tech. Rep.). tech. rep., Stanford University.

Píša, D., Němec, F., Santolík, O., Parrot, M., & Rycroft, M. (2013). Additional attenuation of natural vlf electromagnetic waves observed by the demeter spacecraft resulting from preseismic activity. *Journal of Geophysical Research: Space Physics*, *118*(8), 5286–5295.

Ramos, D., Wilson, G., Sousa, A., Marshall, R., Brunetto, K., Ballenthin, J., ... others (2019). A cubesat receiver for the study of vlf-waves at leo. In *Cubesats* *and smallsats for remote sensing iii* (Vol. 11131, p. 111310P).

Sauvaud, J. A., Maggiolo, R., Jacquey, C., Parrot, M., Berthelier, J.-J., Gamble, R., & Rodger, C. J. (2008). Radiation belt electron precipitation due to VLF transmitters: Satellite observations. *Geophys. Res. Lett.*, *35*, L09101. doi: 10.1029/2008GL033194

Scherbarth, M., Smith, D., Adler, A., Stuart, J., & Ginet, G. (2009). Afrl's demonstration and science experiments (dsx) mission. In *Solar physics and space weather instrumentation iii* (Vol. 7438, p. 74380B).

Shen, X., Zhang, X., Yuan, S., Wang, L., Cao, J., Huang, J., ... Dai, J. (2018). The state-of-the-art of the china seismo-electromagnetic satellite mission. *Science China Technological Sciences*, *61*(5), 634–642.

Spanjers, G., Winter, J., Cohen, D., Adler, A., Guarnieri, J., Tolliver, M., ... Summers, J. (2006). The AFRL demonstration and science experiments (DSX) for DoD space capability in the MEO. In *2006 ieee aerospace conference.*

Starks, M. J., Quinn, R. A., Ginet, G. P., Albert, J. M., Sales, G. S., Reinisch, B. W., & Song, P. (2008). Illumination of the plasmasphere by terrestrial very low frequency transmitters: Model validation. *J. Geophys Res.*, *113*, A09320.

Wang, C. C.-I. (2009). *High fidelity analog-to-digital conversion for spaceborne applications.* Stanford University.

Yau, A. W., & James, H. G. (2011). Scientific objectives of the canadian cassiope enhanced polar outflow probe (e-pop) small satellite mission. In *The sun, the solar wind, and the heliosphere* (pp. 355–364). Springer.

Zhao, S., Zhou, C., Shen, X., & Zhima, Z. (2019). Investigation of vlf transmitter signals in the ionosphere by zh-1 observations and full-wave simulation. *Journal of Geophysical Research: Space Physics*, *124*(6), 4697–4709.

Zhima, Z., Huang, J., Shen, X., Xia, Z., Chen, L., Piersanti, M., ... others (2020). Simultaneous observations of elf/vlf rising-tone quasiperiodic waves and energetic electron precipitations in the high-latitude upper ionosphere. *Journal of Geophysical Research: Space Physics*, *125*(5), e2019JA027574.